Article

Design Methodology of a Power Split Type Plug-In Hybrid Electric Vehicle Considering Drivetrain Losses

Hanho Son, Kyusik Park, Sungho Hwang and Hyunsoo Kim *

School of Mechanical Engineering, Sungkyunkwan University, Suwon-si 16419, Korea; hanho1014@naver.com (H.S.); rbtlr9010@naver.com (K.P.); hsh@me.skku.ac.kr (S.H.)
* Correspondence: hskim@me.skku.ac.kr; Tel.: +82-31-290-7911

Abstract: This paper proposes a design methodology for a power split type plug-in hybrid electric vehicle (PHEV) by considering drivetrain losses. Selecting the input split type PHEV with a single planetary gear as the reference topology, the locations of the engine, motor and generators (MGs), on the speed lever were determined by using the mechanical point considering the system efficiency. Based on the reference topology, feasible candidates were selected by considering the operation conditions of the engine, MG1, and a redundant element. To evaluate the fuel economy of the selected candidates, the loss models of the power electronic system and drivetrain components were obtained from the mathematical governing equation and the experimental results. Based on the component loss model, a comparative analysis was performed using a dynamic programming approach under the presence or absence of the drivetrain losses. It was found that the selection of the operating mode and the operation time of each mode vary since the drivetrain loss affects the system efficiency. In addition, even if the additional modes provide the flexibility of selecting the operating mode that results in a higher system efficiency for the given driving condition, additional drivetrain elements for realizing the modes can deteriorate the fuel economy due to their various losses.

Keywords: design methodology; power split type; plug-in hybrid electric vehicle (PHEV); drivetrain losses; dynamic programming

1. Introduction

To meet the regulations for reducing CO_2 emissions and increasing the fuel economy, the development of electric drive vehicles such as the battery electric vehicle (BEV) and hybrid electric vehicle (HEV) are an inevitable necessity.

The plug-in hybrid electric vehicle (PHEV) has emerged as a viable solution to meet these regulations, while overcoming the disadvantage of the relatively short travel distance of the BEV [1]. PHEV can be driven only using electric energy until the battery state of charge (SOC) decreases to the lower limit, which is called the 'All Electric Range' (AER) or the 'charge depleting (CD) mode'. After AER, PHEV has to run using the internal combustion engine and motor(s) to sustain the battery SOC, which is called the 'charge sustaining (CS) mode'. In CS mode, various operating modes such as series, parallel, etc. are used depending on the PHEV configuration. When the PHEV is operated in CS mode, the fuel economy is directly related to the operating modes, which are determined from its configuration. The PHEV configuration can be classified into series, parallel, and power-split type configurations [2]. The Toyota hybrid system (THS) is a typical example of the input split type configuration in which the engine power is split at the input side. The THS enables the engine to operate on the optimal operating line (OOL) via the electrically continuous variable transmission

function. In addition, the THS has a relatively simple structure without using the clutch and brake to change the mode [3]. However, the power circulation that occurs when the vehicle runs at high speed has been mentioned as a major drawback that deteriorates the fuel economy [4,5]. The THS uses two operating modes; the EV and HEV modes. The number of modes that the PHEV can realize is directly related to the fuel economy because, with a greater number of PHEV modes, more flexibility can be provided for the given driving conditions [6]. On the other hand, additional drivetrain elements, such as the clutch or brake, which are required to implement an additional mode, can cause parasitic loss in the drivetrain.

To develop the PHEV configuration with a high system efficiency, design methodologies or new system configurations have been investigated [7]. To reduce the power circulation, an optimal gear ratio design for the planetary gear and the final reduction gear was proposed [8], and the speed ratio control was investigated to drive the vehicle near the mechanical point [9]. A topology optimization was performed for HEV with transmission to improve CO_2 emission and fuel economy [10]. To implement multi-mode operation in the input split type PHEV, a design methodology to find a feasible design from the possible combinations, using the clutches and brakes, was investigated. For all possible candidates, the fuel economy and driving performance were evaluated using a backward simulator [8,11]. In addition, a comprehensive design methodology was suggested to find the optimal configuration of the input and output-split type HEV in terms of the fuel economy and driving performance, using the clutch topology and gear ratio [12,13].

In the aforementioned studies, there are some limitations; (1) parasitic losses of the drivetrain components, such as the clutch and brake, which are required to realize the new configuration, were neglected and (2) the unloaded loss of the power electronic systems, such as motor and generators (MGs), were not considered. For PHEVs that have relatively short AER, the above factors influence the fuel economy when the vehicle is operated in CS mode.

In this study, a design methodology for a new PHEV configuration was proposed using the input split type as a design reference. Based on the reference topology, feasible candidates were selected by considering the infeasible and redundant conditions. For each candidate, the improvement ratio of the fuel economy was evaluated by dynamic programming, and a comparative study was performed in terms of the positive aspects of the additional mode and negative aspects of the drivetrain loss.

2. Topology Design Based on the Input Power Split Type PHEV

Search for Feasible Topology to Realize the Multi-Mode PHEV

Since power split type PHEV has the advantage of both series and parallel type configurations [4], power split type was selected as a reference topology in design of a new PHEV configuration. In general, the power split type PHEV is designed by combining one engine, two motor-generators (MGs), and multiple planetary gears. In addition, clutches and/or brakes are used to realize the demanded operating modes [8,11]. When we design a new PHEV using multiple planetary gear sets, numerous configurations can be constructed by connecting the power source (engine, MGs) to each shaft of the planetary gears [14,15]. Since it is unrealistic to evaluate all the possible configurations, it is necessary to narrow the variety of choices. In this study, the following constraints were introduced:

(1)   Single planetary gear system:

     Even if multiple planetary gears can provide more freedom than a single planetary gear, additional drivetrain elements such as the clutch and brake are required to connect the planetary gears, and it is difficult to avoid a complicated system structure compared with the single planetary gear system. Also, we can easily deduce that the transmission efficiency of the multiple planetary gear system is lower than that of the single planetary gear system [16]. Furthermore, additional drivetrain elements such as the planetary gear, clutch, and brake may exacerbate the packaging problem, as well as incur increased costs. Therefore, a single planetary gear was selected.

(2)   Input split type:

In the power split transmission (PST) using the single planetary gear (PG), the power is split at the input side or output side of the PST depending on the location of PG [4,17]. The split power flows to the mechanical path and electrical path. Since the efficiency of the electrical path, which consists of the power electronic (PE) system including MG1, MG2, and the inverter, is much lower than that of the mechanical path, the PST efficiency increases as the power ratio of the electrical path decreases. When all the power flows through the mechanical path, the PST efficiency shows the highest value, and this is called the 'mechanical point' (MP) [18].

In the input split type PHEV, the PST efficiency decreases rapidly when the vehicle speed becomes higher than the speed of the mechanical point. This is because power circulation occurs along the electrical path, which causes decreased PST efficiency. In contrast, in the output split type, the power circulation occurs when the vehicle speed is lower than the mechanical point. Therefore, if the vehicle drives mostly in the city (urban dynamometer driving schedule cycle), in other words, at a low to medium speed, it is desirable to use the input split type that has a relatively high efficiency in the low to medium speed region without the power circulation when the mechanical point is positioned at high speed [18].

Considering the above two constraints, the input split configuration using a single planetary gear was selected as a reference topology in development of a new PHEV.

A power split structure can be represented as a generalized single lever model [19]. Figure 1 shows a lever model of the input split type, which involves one engine and two MGs using the single planetary gear. Since the single PG is used, there are three nodes in the lever. Now, we can find a feasible PST configuration as follows:

(a)   If we use MG2 as a main driving motor, it should be connected to the output node. This is because MG2 needs to be operated to propel the vehicle directly in the electric vehicle (EV) mode, as can be observed in most PHEVs.

(b)   In the single PG, the node of the speed lever should be positioned in the order of the sun (S), carrier (C), and ring gear (R), or vice versa from the lever analogy.

(c)   The mechanical point needs to be located at a high vehicle speed to achieve high PST efficiency in the low to medium speed range.

Therefore, we have two possible configurations, as shown in Figure 1. In Figure 1, *i* is the lever distance from the output to the engine and *a* and *b* are the lever distances from the output to MG1 and to MG2, respectively. It is seen from Figure 1 that *b* is equal to zero because MG2 needs to be located at the output from the above condition (a).

Since the electrical power becomes zero at the mechanical point, we can find the speed ratio of the mechanical point under the condition that the speed of MG1 or MG2 is zero. We define the speed ratio (SR) as,

$$\text{SR} = \frac{\omega_e}{\omega_{out}} \, , \tag{1}$$

where ω_e is the engine speed and ω_{out} is the output speed (vehicle speed). From the speed lever in Figure 1, when the speed of MG1 or MG2 is zero, the speed ratio at the mechanical point is obtained as

$$\text{SR} = \frac{a-i}{a} = \frac{(a/i)-1}{(a/i)} \text{ at mechanical point.} \tag{2}$$

In Figure 2, the speed ratio at the mechanical point is shown with respect to a/i for an input split type transmission [20]. To meet condition (c) above, the speed ratio at the mechanical point should be the overdrive ratio (region F) for which the output speed of the PST is higher than the input (engine) speed. This implies that the lever distances *a* and *i* need to be in the same direction and that a/i is larger than one. It is found that lever A satisfies the aforementioned requirements, while lever

B does not meet the requirements. In addition, it is found that the engine needs to be located at the center node of lever A, i.e., at carrier C, since the order of the PG node should be S, C, R or R, C, S (from condition (b)).
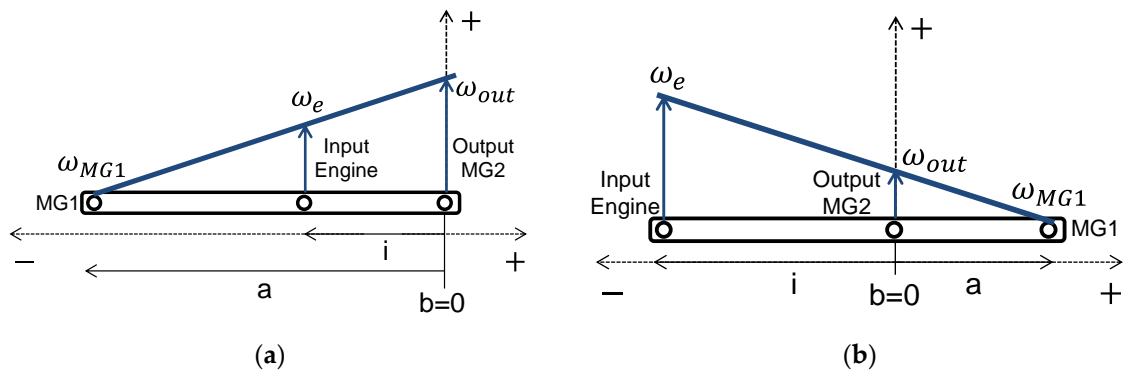

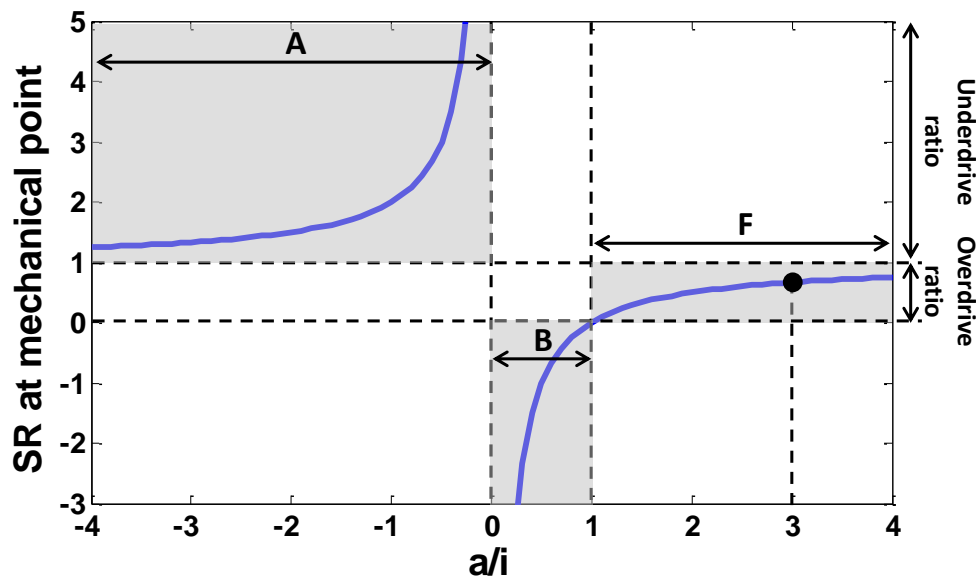**Figure 1.** A generalized single lever model for the input split plug-in hybrid electric vehicle (PHEV). (**a**) Lever A; (**b**) Lever B.

Figure 2. Speed ratio at the mechanical point [20].

Now, we determine the position of MG2 (output). MG2 can be located at the sun gear, S (Figure 3a), or the ring gear, R (Figure 3b). From the speed lever analogy, it is found that MG2 is positioned at the ring gear when a/i is greater than 2; meanwhile it is positioned at the sun gear for $1 < a/i < 2$.

From the lever analogy of the speed and torque, we can obtain the power of each node using a/i. Defining the power ratio PR as the ratio of the MG1 power (electrical power) to the engine (input) power, the power ratio is represented as

$$\text{PR} = \frac{P_{MG1}}{P_e} = \frac{\omega_{out}}{\omega_e}\left(\frac{1}{(a/i)-1}\right) + 1 \tag{3}$$

In Figure 4, the power ratio is shown for a/i between 1 and 3.5 when the engine speed is 1500 rpm, the engine torque is 100 Nm, and the output speed is 2000 rpm. It is seen from Figure 4 that the power ratio decreases as a/i increases. Since the PST efficiency increases as the power ratio decreases, in other words, the power through MG1 (electrical path) decreases, we find that MG2 needs to be positioned at the ring gear.
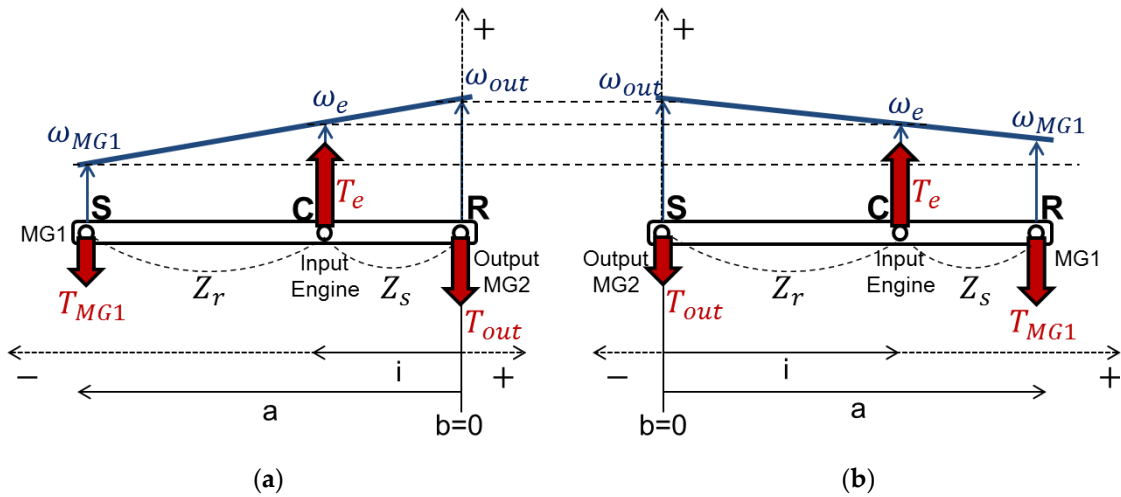
Figure 3. Lever analysis for the input split type by a/i. (**a**) a/i is larger than 2; (**b**) a/i is smaller than 2.
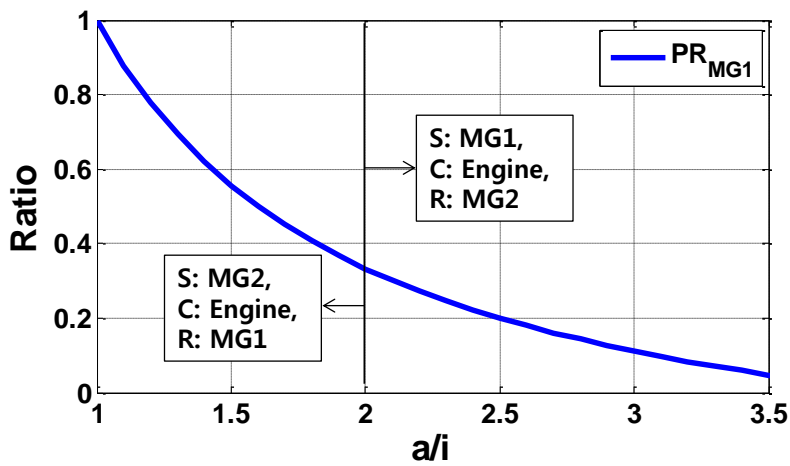

Figure 4. Speed, torque, and power ratio versus a/i when ω_e = 1500 rpm, T_e = 100 Nm, ω_{out} = 2000 rpm.

In Figure 5, a schematic diagram of the input split type PST using the single PG is shown, which is selected from the design procedure. The PST in Figure 5 consists of one engine at the carrier (C), MG2 at the ring gear (R), and MG1 at the sun gear (S). The PST in Figure 5a provides two operating modes when driving; (1) electric vehicle (EV) and (2) power split mode. In the EV mode, the vehicle is propelled by MG2 using electric energy (Figure 5b). In the power split mode, the engine power is split at the PG and transmitted to MG1 and to the output (Figure 5c). At this moment, the power may circulate through the closed path, depending on the vehicle speed.

Using the PST in Figure 5 as a reference topology, a design methodology of the PHEV that can realize more operating modes with high efficiency is investigated.

To realize more than two operating modes, the degree of freedom of the single PG needs to be changed using the clutch and brake. In Figure 6a, the possible positions where the clutch and brake can be added are shown. Since the PG has three nodes (sun, carrier, and ring gear), the clutches, CL1, CL2, CL3, and the brakes, BK1, BK2, and BK3, can be added at each node, as shown in Figure 6a [11,15]. Mathematically, the number of combinations that can be constructed from three clutches and three brakes is 2^6. However, infeasible combinations can be eliminated by considering the real driving environment. In the power split mode, in other words, in the hybrid electric vehicle (HEV) mode in

which the engine and MG2 work together, the engine and MG1 should always operate together due to the following reasons:

(1)   The engine needs to supply the power to propel the vehicle and to generate MG1.
(2)   When the engine works, MG1 is required to control the engine operation on the OOL.

From the above constraints, it is seen that clutches CL2 and CL3 should always be engaged, which means that CL2 and CL3 are not necessary, as shown Figure 6b. Therefore, the number of combinations becomes 2^4(=16) by eliminating CL2 and CL3.
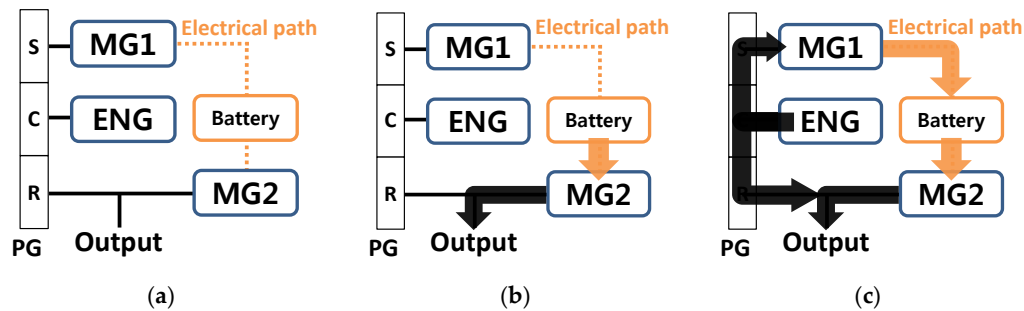

(a)   (b)   (c)

Figure 5. Reference power split transmission. (**a**) Input split power split transmission (PST); (**b**) electric vehicle (EV) mode; (**c**) Power split mode.
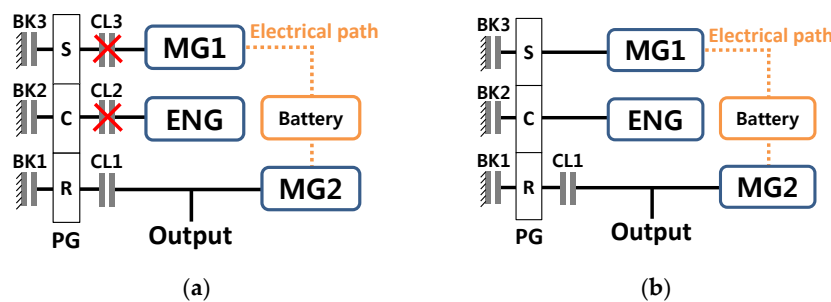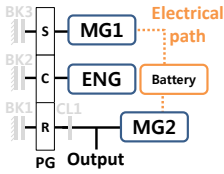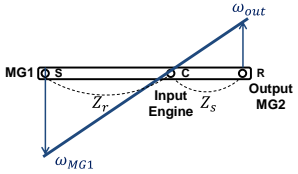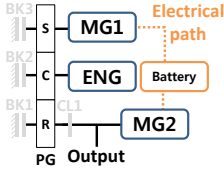

(a)   (b)

Figure 6. Schematic diagram for the reference topology. (**a**) All possible locations for adding the clutch and brake [11]; (**b**) Feasible locations for adding the clutch and brake.

By adding CL1, BK1, BK2, and BK3 to the reference topology, the following modes can be realized:

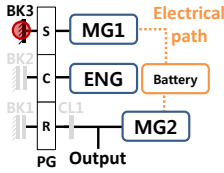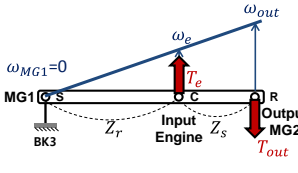|	
EV#1:	The vehicle is propelled only by MG2. MG1 and the engine are off. No clutch or brake is required.
Power split:	This mode can be implemented as explained in Figure 5c. No additional clutch or brake is needed from the reference topology.
EV#2:	MG2 and MG1 propel the vehicle together. Since the engine does not work, the reaction force acting on the carrier must exist to transmit the MG1 torque through the PG. Therefore, the carrier is fixed by activating BK2.
Parallel:	The engine and MG2 propel the vehicle using the parallel path. MG1 does not function, which requires BK3 to make the MG1 speed zero. The engine power is transmitted to the output through the mechanical path without using the electrical path. MG2 works using the battery energy.
Series:	To implement this mode, the engine needs to be separated from the output, which requires CL1 to disengage the power from the engine and BK1 to ground the ring gear. The engine only drives MG1 to generate the electrical power, which is transmitted to the output through the electrical path.

In Table 1, the operation of the clutch and brake, the lever analogy, and the speed and torque equation for each mode are shown. It is seen from Table 1 that EV#1 and power split mode are implemented as a basic operating mode without any additional elements. For the EV#2 mode, BK2 is required; meanwhile BK3 is required for the parallel mode. Finally, it is noted that BK1 and CL1 are needed for the series mode.

Table 1. Possible operating modes with the speed and torque equation.

Operating Mode	Lever Analogy	Speed and Torque Equation ($N_{PG} = Z_r/Z_s$)
EV#1		$\begin{bmatrix} \omega_{MG1} \\ \omega_{MG2} \end{bmatrix} = \begin{bmatrix} N_{PG} & 0 \\ 1 & 0 \end{bmatrix} \begin{bmatrix} \omega_{out} \\ \omega_e \end{bmatrix}$ $[T_{out}] = \begin{bmatrix} 0 & 0 & 1 \end{bmatrix} \begin{bmatrix} T_{MG1} \\ T_e \\ T_{MG2} \end{bmatrix}$
Power split		$\begin{bmatrix} \omega_{MG1} \\ \omega_{MG2} \end{bmatrix} = \begin{bmatrix} -N_{PG} & 1+N_{PG} \\ 1 & 0 \end{bmatrix} \begin{bmatrix} \omega_{out} \\ \omega_e \end{bmatrix}$ $[T_{out}] = \begin{bmatrix} 1 & 1 & 1 \end{bmatrix} \begin{bmatrix} T_{MG1} \\ T_e \\ T_{MG2} \end{bmatrix}$
EV#2		$\begin{bmatrix} \omega_{MG1} \\ \omega_{MG2} \end{bmatrix} = \begin{bmatrix} N_{PG} & 0 \\ 1 & 0 \end{bmatrix} \begin{bmatrix} \omega_{out} \\ \omega_e \end{bmatrix}$ $[T_{out}] = \begin{bmatrix} N_{PG} & 0 & 1 \end{bmatrix} \begin{bmatrix} T_{MG1} \\ T_e \\ T_{MG2} \end{bmatrix}$
Parallel		$\begin{bmatrix} \omega_{MG1} \\ \omega_{MG2} \end{bmatrix} = \begin{bmatrix} 0 & 0 \\ 1 & 0 \end{bmatrix} \begin{bmatrix} \omega_{out} \\ \omega_e \end{bmatrix}$ $[T_{out}] = \begin{bmatrix} 0 & 1+N_{PG} & 1 \end{bmatrix} \begin{bmatrix} T_{MG1} \\ T_e \\ T_{MG2} \end{bmatrix}$
Series		$\begin{bmatrix} \omega_{MG1} \\ \omega_{MG2} \end{bmatrix} = \begin{bmatrix} 0 & 1+N_{PG} \\ 1 & 0 \end{bmatrix} \begin{bmatrix} \omega_{out} \\ \omega_e \end{bmatrix}$ $[T_{out}] = \begin{bmatrix} 0 & 0 & 1 \end{bmatrix} \begin{bmatrix} T_{MG1} \\ T_e \\ T_{MG2} \end{bmatrix}$
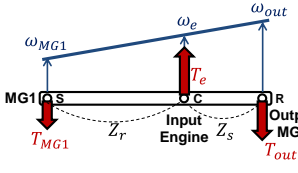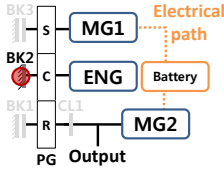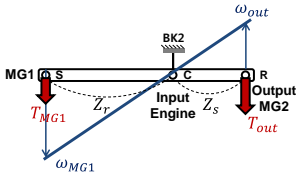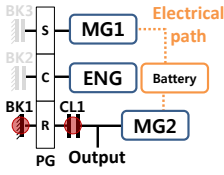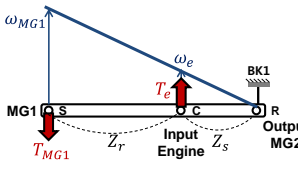
In Table 2, sixteen candidates are shown with the operating mode and additional element(s). It is seen from Table 2 that some of the candidates have a redundant element when realizing the target operating modes. For example, candidate #14 can realize the EV#1, power split, EV#2, and parallel mode only by using BK2 and BK3 without CL1. Therefore, CL1 is a redundant element, and it is found that candidate #14 is equivalent to candidate #11. Similarly, candidate #15 is equivalent to #11, #2 and #3 are equivalent to #1, etc. After eliminating the candidates that have a redundant element (gray rows), eight candidates were selected, as shown in Figure 7.

Table 2. All feasible candidates to realize multi-mode PHEV.

Candidate No.	Additional Element	Operating Mode	Redundant Element	Equivalent Candidate
#1	Reference	Basic (EV#1, Power split)	-	-
#2	CL1	Basic	CL1	#1
#3	BK1	Basic	BK1	#1
#4	BK2	Basic + EV#2	-	-
#5	BK3	Basic + Parallel	-	-
#6	CL1, BK1	Basic + Series	-	-
#7	CL1, BK2	Basic + EV#2	CL1	#4
#8	CL1, BK3	Basic + Parallel	CL1	#5
#9	BK1, BK2	Basic + EV#2	BK1	#4
#10	BK1, BK3	Basic + Parallel	BK1	#5
#11	BK2, BK3	Basic + EV#2, Parallel	-	-
#12	CL1, BK1, BK2	Basic + EV#2, Series	-	-
#13	CL1, BK1, BK3	Basic + Parallel, Series	-	-
#14	CL1, BK2, BK3	Basic + EV#2, Parallel	CL1	#11
#15	BK1, BK2, BK3	Basic + EV#2, Parallel	BK1	#11
#16	CL1, BK1, BK2, BK3	Basic + EV#2, Parallel, Series	-	-
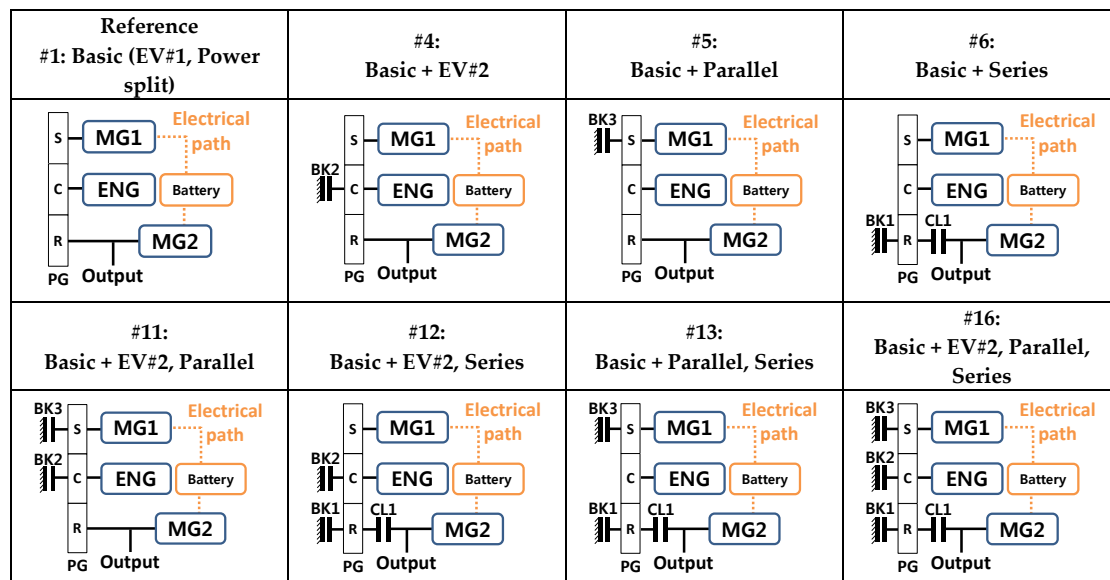
Figure 7. Eight candidates with operating modes.

3. Component Loss Model

As shown in Figure 7, eight candidates for new PHEV configurations were obtained using the additional clutch and brake. In general, it is expected that, as the number of the operating modes increases, the fuel economy increases, since the PHEV can be operated with high efficiency by selecting the proper operating mode for the given wheel torque and speed. However, additional drivetrain components such as the clutch and brake cause parasitic power loss. Therefore, the pros and cons of the multi-mode operation need to be evaluated when adding the operating mode.

In this study, to evaluate the effect of the power electronic (PE) loss and drivetrain loss on the fuel economy, the component loss models were obtained based on the mathematical governing equation and experimental results.

3.1. PE Loss

The MG1 and MG2 losses were calculated from the efficiency map. The efficiency of MG1 or MG2 can be determined from the operation point for the given torque and speed (Figure 8a,b). The high-voltage DC/DC converter (HDC) boosts the battery voltage in consideration of the operating conditions of MG1 or MG2. When the HDC boosts the battery voltage, a boost loss occurs. The HDC loss was determined from the HDC efficiency with respect to the battery power (Figure 8c). In addition, the battery loss was obtained from the charge (discharge) efficiency. In this study, the battery charge (discharge) efficiency was assumed to be 98.5% [21].
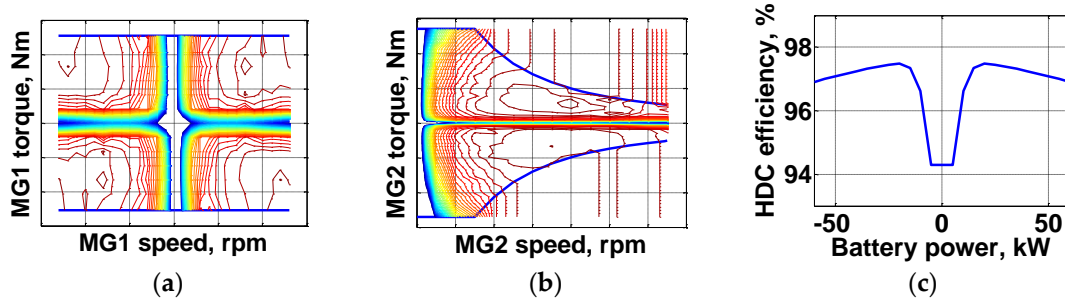

Figure 8. The efficiency map derived from the experimental result for: (**a**) motor generator 1 (MG1); (**b**) MG2; (**c**) high-voltage DC/DC converter (HDC).

3.2. Drivetrain Loss

The drivetrain losses have been described in detail in the literature [22]. A short summary of the drivetrain losses is as follows:

Gear loss: Gear loss was assumed to be 1% of the transmitted torque [23], which is widely used in the automotive industry.

Planetary gear loss: When the sun, pinion, and ring gear are meshing, the planetary gear loss occurs due to the gear teeth friction. The planetary gear loss is represented as [24,25]:

$$T_{loss\_PG} = \begin{cases} k_{PG} \times T_{in\_PG}, & \text{when the carrier is fixed} \\ k_{PG} \times \left(\frac{Z_r}{Z_r + Z_s} \right) \times T_{in\_PG}, & \text{when the ring gear is fixed} \\ k_{PG} \times \left(\frac{Z_s}{Z_r + Z_s} \right) \times T_{in\_PG}, & \text{when the sun gear is fixed,} \end{cases} \tag{4}$$

where T_{loss} is the torque loss, T_{in} is the input torque, and k is the coefficient of friction for PG.

Bearing loss: There are loaded and unloaded losses in the bearing. Loaded loss is proportional to the bearing load. The loaded loss is calculated as follows [26,27]:

$$T_{loss\_BRGload} = f_1 \times P_1{}^a \times d_m{}^b \times 10^{-3}, \tag{5}$$

where a, b, and f_1 are the coefficients according to the bearing type, P_1 is the equivalent bearing load and is determined from the axial and radial bearing reaction force, and d_m is the bearing mean diameter.

Bearing unloaded loss is caused by the slip between the rotating surface and the lubrication oil film. The bearing unloaded loss is represented as

$$T_{loss\_BRGunload} = \begin{cases} 1.6 \times 10^{-8} \times f_0 \times d_m{}^3, & \text{if } (v_{oil} \times n) < \frac{2000 \text{ mm}^2}{s \cdot min} \\ 10^{-10} \times f_0 \times (v_{oil} \times n)^{\frac{2}{3}} \times d_m{}^3, & \text{if } (v_{oil} \times n) \geq \frac{2000 \text{ mm}^2}{s \cdot min}, \end{cases} \tag{6}$$

where f_0 is the coefficient for the bearing unloaded loss, v_{oil} is the kinematic viscosity, and n is the bearing rotational speed.

Churning loss: To reduce friction between the gear teeth, the final reduction gear rotates in lubrication oil. During the gear rotation, the churning loss occurs in proportion to the rotational speed. Churning loss is calculated as follows [28]:

$$T_{loss\_churning} = \frac{1}{2}\rho\omega^2 R_p{}^3 S_m C_m,$$ (7)

where ω is the rotational speed, ρ is the lubricant density, R_p is the gear pitch effective radius, S_m is the contact surface coefficient, and C_m is the dimensionless churning torque loss.

Brake and clutch loss: The brake and clutch unloaded losses are the drag losses between the friction surface and lubricant in the disengaged state. The brake and clutch unloaded losses were modeled using the experimental results (Figure 9a).

MG1 unloaded loss: MG1 unloaded loss is caused by the mechanical and electrical components when MG1 rotates freely [29]. For the input split type, MG1 does not produce the power to propel the vehicle in the EV#1 mode and is freely rotating because it is connected to the vehicle through the planetary gear. MG1 unloaded loss was modeled using the experimental results (Figure 9b).

Oil pump loss: The oil pump provides a flow rate for the lubrication, cooling, and the control of the clutch and brake. Since a mechanical oil pump, which is driven by the driveshaft via a gear was used in this study, the oil flow is supplied in proportion to the vehicle speed. While the clutch or brake is engaged, additional oil flow is needed to generate the control pressure. Therefore, the oil pump loss depends on the vehicle speed and control pressure. In this study, the oil pump loss was obtained from Prius THS experimental results, shown in Figure 9c [16].
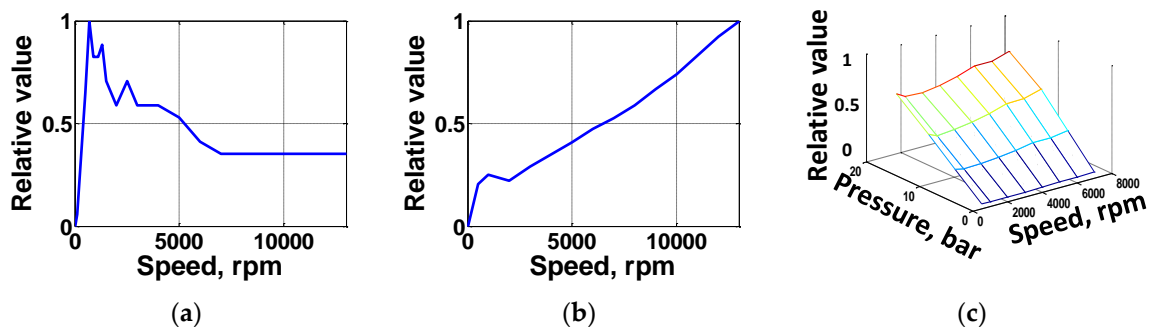

Figure 9. The torque loss map derived from the experimental result for: (**a**) Brake/clutch; (**b**) MG1 unloaded; (**c**) Oil pump.

To calculate the drivetrain loss, the design specification and location of each element are required. In Figure 10, a schematic diagram of the reference PHEV, using the design concept described in Figure 6b, is shown. The installation positions of the bearings were determined referring to the 3rd generation Toyota Prius. The bearing losses inside the MG1 and MG2 were considered in the motor efficiency map. MG2 was connected to the output through two reduction gears, G1-G2 and G3-G4. The friction face area of the brake and clutch and the number of clutch friction faces were determined by considering the transmitted torque [30].

The magnitude of the PE loss and drivetrain loss vary depending on the power flow path, which is determined by the operating mode. In Table 3, the components of the PE loss and drivetrain loss are shown for each operating mode.

In EV#1 and parallel mode, the PE losses occur from the battery charge/discharge, MG2, and HDC operation. The MG1 loss needs to be considered in the EV#2 mode, power split, and series mode, in addition to the battery, MG2, and HDC losses. The drivetrain losses come from the gear, planetary gear, and bearings. The unloaded losses occur due to the drag when the clutch or brake is freely rotating. The churning loss always exists at the final reduction gear. In addition, the oil pump loss needs to be considered when the clutch or brake is engaged.
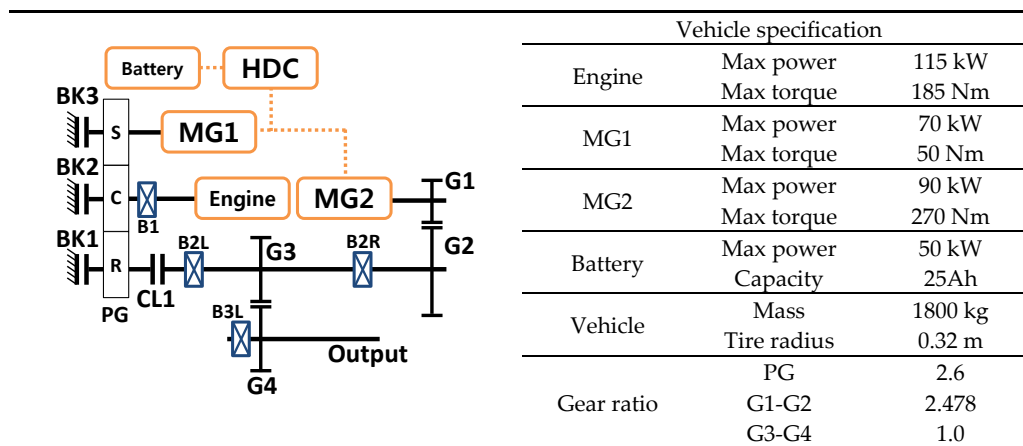
Vehicle specification		
Engine	Max power	115 kW
	Max torque	185 Nm
MG1	Max power	70 kW
	Max torque	50 Nm
MG2	Max power	90 kW
	Max torque	270 Nm
Battery	Max power	50 kW
	Capacity	25Ah
Vehicle	Mass	1800 kg
	Tire radius	0.32 m
Gear ratio	PG	2.6
	G1-G2	2.478
	G3-G4	1.0

Figure 10. Reference topology and specifications with drivetrain elements and additional clutch and brakes. MG: motor and generator, CL#: clutch, PG#: planetary gear, B#L: bearing on left side, B#R: bearing on right side, HDC: high voltage DC/DC converter, BK#: brake, G#: gear.

Table 3. Power electronics (PE) and drivetrain loss for each operating mode.

Operating Mode		EV#1	EV#2	Power Split	Parallel	Series
PE loss		Battery, HDC, MG2	Battery, HDC, MG2, MG1	Battery, HDC, MG2, MG1	Battery, HDC, MG2	Battery, HDC, MG2, MG1
Drivetrain loss	Loaded	Gear, BRG	Gear, BRG, PG	Gear, BRG, PG	Gear, BRG, PG	Gear, BRG, PG
	Un-loaded	BRG, Churning, MG1 unloaded, BK#	BRG, Churning, BK#, Pump	BRG, Churning, BK#	BRG, Churning, BK#, Pump	BRG, Churning, BK#, CL1, Pump

4. Backward Simulator Using Dynamic Programming

To evaluate the maximum potential in the fuel economy of the eight candidates in Figure 7, a backward simulator was developed using dynamic programming (DP). Since DP is able to find the optimal SOC trajectory regardless of the control strategy, which guarantees minimum fuel consumption for the given PHEV configuration [31,32], it was used for the comparative analysis of the candidates for the presence or absence of the drivetrain losses.

The PHEV system in Figure 7 has two control variables, engine speed and torque, and one state variable, battery SOC [33]. For each time step, $k - 1$, the instantaneous optimal operating point of the engine is determined for the specific battery power. When the operating point of the engine is given, the PE loss and drivetrain loss are calculated [22]. Considering the component loss, the optimal fuel consumption rate, g_{k-1}, is obtained through the instantaneous optimization process.

After the process is completed, global optimization is performed to find the minimum fuel consumption over the whole driving cycle. The global optimization process can be represented as a recursive equation [33,34]. The recursive equation and constraint are represented as

$$\text{Recursive equation}: J_k^*(SOC_k) = \{g_{k-1}(\omega^e_{k-1}, T^e_{k-1}) + J_{k-1}^*(SOC_{k-1})\}$$
$$\text{Constraint}: SOC_{initial} - SOC_{final} = 0, \tag{8}$$

where k is the discrete time step, J_k^* is the minimum fuel consumption from 1 to k step, J_{k-1}^* is the minimum fuel consumption from 1 to $k - 1$ step, ω^e_{k-1} and T^e_{k-1} are respectively the speed and torque of the engine that has the minimum fuel consumption rate at the $k - 1$ step, and g_{k-1} is the fuel consumption rate at the $k - 1$ step.

Using the recursive equation, we can find the minimum fuel consumption, J_k^*; in other words, the maximum potential in the fuel economy over the whole driving schedule [35,36].

5. Comparative Analysis Using Dynamic Programming

PE Loss and Drivetrain Loss

To evaluate the influence of the drivetrain losses on the fuel economy, simulation was performed for candidate #16 using the backward simulator, in which the target PHEV undergoes the highway fuel economy test (HWFET) cycle. In the simulation, the final battery SOC was assumed to be equal to the initial SOC. As described in Section 4, the operation points of the engine, MG1, and MG2 were determined, which guarantee the minimum fuel consumption by the dynamic programming results. In addition, the operating mode that provides the minimum fuel consumption was selected.

In Figure 11, the simulation results are shown. The engine torque (b) and speed (c) were almost maintained at the optimal operating point at 80 Nm and 1600 rpm, where the engine has the highest thermal efficiency for the demanded engine power. The MG2 torque (b) showed a negative value when regenerative braking was performed. The battery SOC (d) decreased from the initial value when the vehicle accelerated and increased during the regenerative braking. The vehicle started in the EV#1 mode and used the EV#2, power split, parallel, and regenerative braking modes (e) during the driving. It is seen that the parallel mode was mostly used for the HWFET cycle, while the series mode was never used.
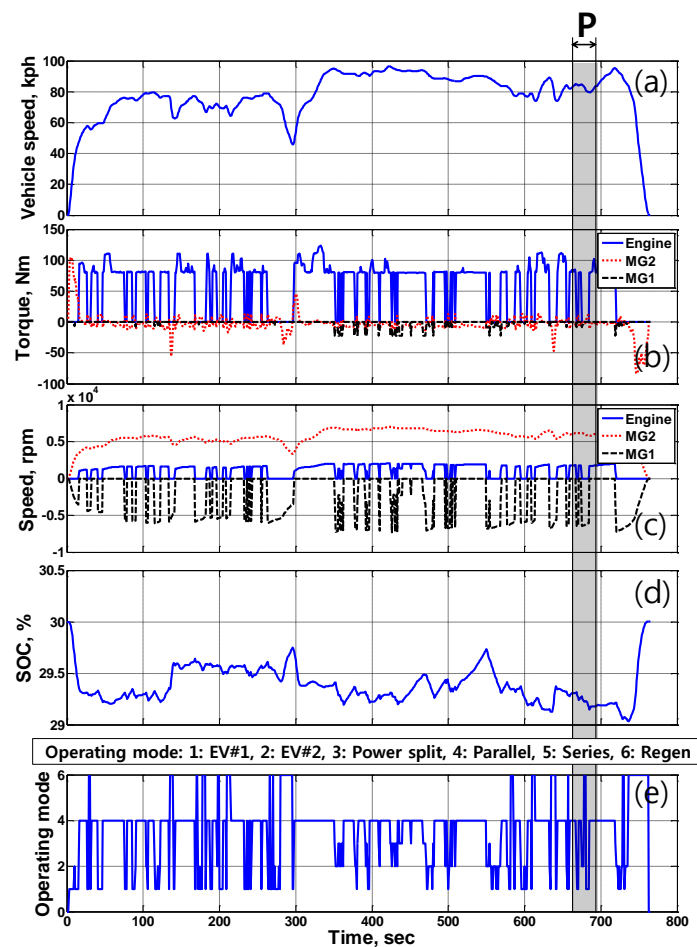

Figure 11. Backward simulation result for candidate #16 considering PE and drivetrain loss (highway fuel economy test (HWFET) cycle). (**a**) Vehicle speed; (**b**) Torque; (**c**) Speed; (**d**) Battery SOC; (**e**) Operating mode.

In Figure 12, the drivetrain loss and PE loss in region P (t = 665–695 s) of Figure 11 are shown. The gear (9–150 W), bearing (150–200 W), and PG losses (3–210 W) (Figure 12a) always occur when the vehicle drives. The gear and PG losses showed an almost zero value at an instant when the transmitted torque is very small during regenerative braking. An MG1 unloaded loss of 400 W occurred when MG1 was freely rotating, such as in the EV#1 and regenerative braking mode. When MG1 works, the MG1 unloaded loss does not appear. Instead, the PE loss of MG1 occurs (c). The drag losses of BK1, BK2, and BK3 (b) were 20–45 W when they were disengaged. In region P, since the series mode was not used (e), BK1 was disengaged and CL1 was engaged, causing a drag loss of BK1 of 30 W and a zero drag loss of CL1. The BK2 loss was zero in the EV#2 mode when it was engaged but showed a 20 W loss in the parallel mode when it was disengaged. It is seen that a drag loss of 45 W occurred in BK3 when BK3 was disengaged. In addition, a pump loss (b) of 45 W occurred, supplying the pressure for the engagement of BK and CL1. In Figure 12c, the PE losses are shown. The MG2 loss of 400–900 W occurred because MG2 always works when the vehicle drives. The MG1 loss (500–700 W) occurred in the EV#2 mode. The HDC loss showed a range of 0–50 W. In Figure 12d, the total drivetrain loss is shown with the PE loss. It is seen that the total drivetrain loss (300–900 W) was almost the same as the PE loss (385–1260 W), which demonstrates that drivetrain loss should be considered when evaluating the fuel economy for a new PHEV configurations.
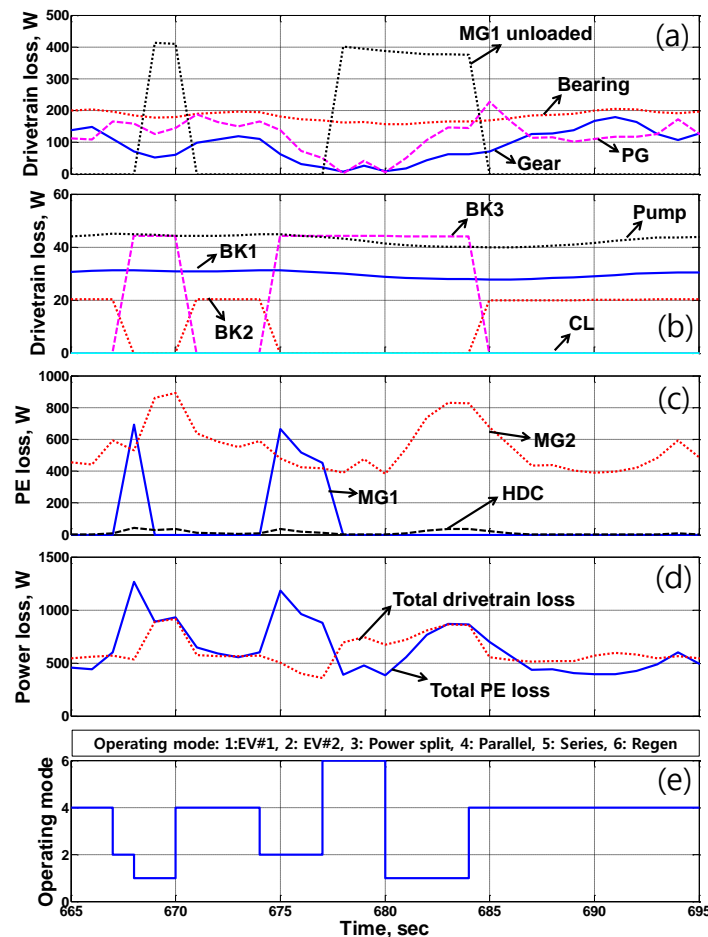
Figure 12. PE and drivetrain loss for candidate # 16 when driving the HWFET cycle (665–695 s). (**a**,**b**) Drivetrain loss; (**c**) PE loss; (**d**) Power loss; (**e**) Operating mode.

In Figure 13a,b, the operating modes are plotted, which provide the minimum fuel consumption for the demanded wheel power and vehicle speed. The operating mode was selected from the global optimization using dynamic programming. It is seen from the dynamic programming results that the

PHEV (candidate #16) does not use the EV#2 and series mode without consideration of the drivetrain loss, even if it can implement the EV#2 and series mode. This is because these two operating modes cannot provide the minimum fuel consumption for the given driving condition. Instead, the EV#1, power split and parallel mode were used with the operation times of 283 s, 27 s, and 365 s, respectively, across the total driving time of 765 s (Figure 13c). On the other hand, when the drivetrain loss is considered, as can be seen from Figure 13b,c, the EV#2 mode is used at low wheel power (less than 8 kW) and high vehicle speed (72–95 kph). The operation time of the EV#2 mode is 79 s, while the EV#1, power split, and parallel modes are used for 110 s, 30 s, and 456 s, respectively. It is noted that the series mode was not used, even when drivetrain loss was considered.

From the comparative analysis, it was found that the mode selection and operation time of each mode varies depending on the presence or absence of drivetrain loss. This is because the drivetrain loss affects the system efficiency for the given driving conditions. As a result, a different operating mode was selected and a different mode operation time was obtained, which leads to a different fuel economy. When the drivetrain loss is not considered, the fuel economy was obtained as 28.76 km/L, and when the drivetrain loss is taken into consideration, the fuel economy is decreased by as much as 8.1% to 26.43 km/L. It is seen from the comparative analysis for candidate #16 that the drivetrain loss has a significant impact on the fuel economy, which demonstrates that the drivetrain loss should be considered in fuel economy evaluations.

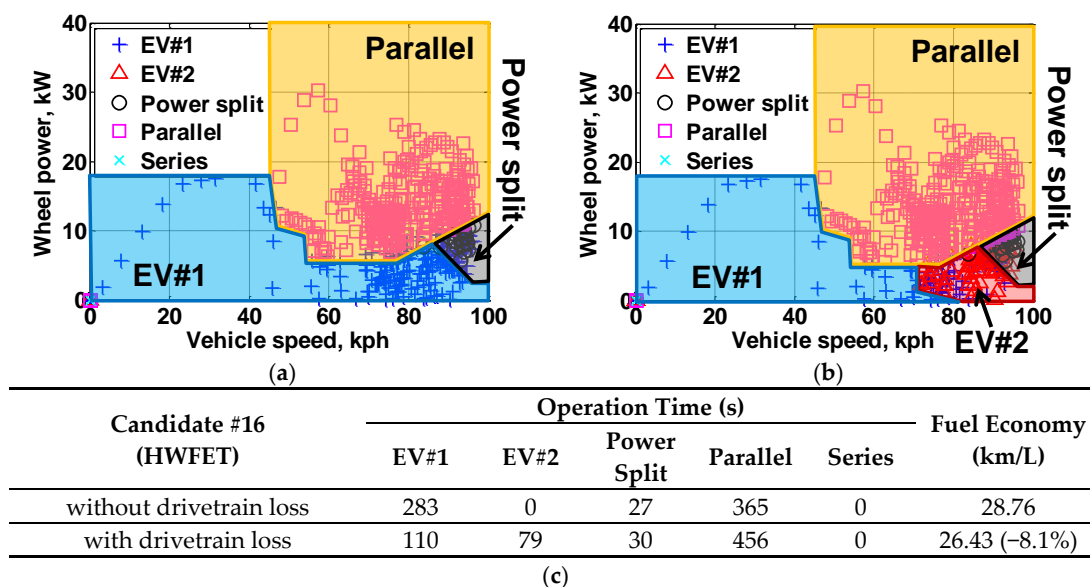| Candidate #16 (HWFET)	Operation Time (s)					Fuel Economy (km/L)
	EV#1	EV#2	Power Split	Parallel	Series	
without drivetrain loss	283	0	27	365	0	28.76
with drivetrain loss	110	79	30	456	0	26.43 (−8.1%)

(c)

Figure 13. Comparison of optimal operating mode for candidate #16 in the presence or absence of drivetrain losses (HWFET). (**a**) Without drivetrain loss; (**b**) With drivetrain loss; (**c**) Operation time and fuel economy.

Now, considering the drivetrain loss, the fuel economies of the eight candidates in Figure 7 were evaluated. In Table 4, simulation results of the operation time, fuel economy, PE loss, and drivetrain loss are compared for the HWFET cycle when the vehicle is operated in CS mode.

It is seen from Table 4 that the fuel economies of candidates #6 and #12 were decreased compared with the reference (candidate #1) in spite of the additional modes. This is because brake drag and pump loss occurred from the additional elements, BK1, BK2, and CL1. The fuel economies of candidates #5, #11, #13, and #16 were improved by 3.65%–4.04%, and we found that all these candidates have the parallel mode in common. It is seen that the operation time of the parallel mode is 437–456 s, which replaced most of the power split mode operation. The reason why the fuel economy was improved when adding the parallel mode can be explained by the reduced PE loss. In the parallel mode, MG1 is turned off and there is no power flow through the electrical path, which provides a smaller PE loss

than that of the power split mode. As a result, candidates #5, #11, #13, and #16, which can implement the parallel mode, have smaller PE loss (524.3–540.1 kJ) than the other candidates (935–950 kJ). It is also noted that the fuel economy improvement (3.77%) of candidate #16 is less than that of candidate #11 (4.04%), even if it can implement one more operating mode than candidate #11; this is because the drivetrain loss was increased due to the additional elements, BK1 and CL1.

From Table 4, we can select candidate #11 as a new PHEV configuration that provides the best fuel economy using the EV#1, EV#2, power split, and parallel modes.

As shown in the design procedure, which considers the speed and torque lever analogy, drivetrain loss, and PE loss, it is seen that the design methodology proposed in this study can be used effectively for the development of a new PHEV configuration and that the drivetrain losses must be included in the fuel economy evaluation.

Table 4. Fuel economy and component losses of eight candidates for HWFET when the vehicle is operated in charge sustaining (CS) mode.

Candidate		#1 Basic (EV#1, Power Split)	#4 Basic + EV#2	#5 Basic + Parallel	#6 Basic +Series	#11 Basic + EV#2, Parallel	#12 Basic + EV#2, Series	#13 Basic + Parallel Series	#16 Basic + EV#2, Parallel, Series
Additional element		-	BK2	BK3	BK1, CL1	BK2, BK3	BK1, BK2, CL1	BK1, BK3, CL1	BK1, BK2, BK3, CL1
No. of modes		2	3	3	3	4	4	4	5
Operation time (s)	EV#1	89	64	169	89	118	60	172	110
	EV#2	X	45	X	X	69	47	X	79
	Power split	586	566	69	586	33	568	61	30
	Parallel	X	X	437	X	455	X	442	456
	Series	X	X	X	0	X	0	0	0
FE (km/L)		25.47	25.47	26.47 (+3.92%)	25.37 (−0.39%)	26.5 (+4.04%)	25.36 (−0.43%)	26.4 (+3.65%)	26.43 (+3.77%)
PE loss (kJ)	MG2	658.2	645.5	486.1	658.1	463	645.1	485.7	460.3
	MG1	264.1	290.4	15.2	265.9	49.4	292.7	13.3	55
	HDC	12.6	11.5	25.3	12.3	25.2	11.7	25.3	24.8
Total PE loss (kJ)		934.9	947.4	526.6	936.3	537.6	949.5	524.3	540.1
Drivetrain loss (kJ)	MG1-unload	49.7	41.1	80.6	50	60.4	39.7	81.5	57.3
	PG	182.6	175.7	129	182.1	122.4	175.4	128.1	121.6
	Gear	182.3	182.3	182.3	182.3	182.3	182.3	182.3	182.3
	Bearing	133.1	133.1	133.1	133.1	133.1	133.1	133.1	133.1
	CL1 & BK#	0	10.6	25.1	20.4	34.7	31	33.3	42.5
	Pump	18.3	19	25.5	30.9	27	30.9	30.9	30.9
Total drivetrain loss (kJ)		566	561.8	575.6	598.8	559.9	592.4	589.2	567.7

6. Conclusions

A design methodology of a power split type PHEV was proposed by considering the drivetrain losses. As a design reference, an input split type PHEV using a single planetary gear was selected. First, to determine the engine position on the speed lever of the single planetary gear, the mechanical point (MP) at which the power split transmission (PST) has the highest efficiency was investigated with respect to the speed ratio, and it was found that the engine should be located at the carrier to have the MP at high speeds, which provided a higher PST efficiency in the main driving range. In addition, the positions of MG1 and MG2 on the speed lever were determined, which provides a better PST efficiency by reducing the power that flows through the electrical path. Based on the reference topology, feasible locations of the additional clutch and brake were investigated to realize the multi-mode in addition to the basic operating mode of the reference PST. Among the mathematically

possible combinations of 2^6 candidates, sixteen candidates were selected by considering the operation condition of the engine and MG1 in a real driving environment, and, finally, eight candidates were obtained by eliminating the candidates that had a redundant element. To evaluate the fuel economy of the selected candidates, the loss models of the power electronic system (MG1, MG2, HDC) and drivetrain components (gear, planetary gear, clutch, brake, bearing, MG1 unloaded loss, etc.) were obtained based on the mathematical governing equation and experimental results. Based on the component loss model, a backward simulator was developed using dynamic programming to find the maximum potential for the fuel economy of the PHEV candidates for the given driving duty cycle. Using the backward simulation, a comparative analysis was performed under the presence or absence of the drivetrain losses, and it was found that the selection of the operating mode and the operation time of each mode vary, since the drivetrain losses affect the system efficiency. The fuel economy also decreased by as much as 8.1% for the HWFET cycle.

In addition, it was found from the comparative analysis that, even if the additional modes result in flexibility when selecting the operating mode, thus providing a higher system efficiency for the given wheel power and vehicle speed, additional drivetrain elements to realize the modes can deteriorate the fuel economy due to the losses of the additional elements. It is also noted that the series mode was never used due to its low system efficiency. On the other hand, the parallel mode can improve the system efficiency since the PE loss is reduced compared with the other modes.

It is expected that the design methodology proposed in this study, which considers the drivetrain losses, can be used in development of new PHEV configurations.

Author Contributions: Hanho Son developed the design methodology of a power split type PHEV considering drivetrain losses and wrote the paper. Kyusik Park developed the individual models of the target PHEV powertrain and drivetrain losses. Hyunsoo Kim and Sungho Hwang supervised this research and wrote the paper.

Conflicts of Interest: The authors declare no conflict of interest.

References

1. U.S. DOE. Chapter 8: Advanced Clean Transportation and Vehicle Systems and Techonologies, Quadrennial Technology Review 2015. Available online: https://energy.gov/sites/prod/files/2016/01/f28/QTR2015-8E-Plug-in-Electric-Vehicles.pdf (accessed on 11 January 2017).
2. Ehsani, M.; Gao, Y.; Gay, S.; Emadi, A. *Modern Electric, Hybrid Electric, and Fuel Cell Vehicles*, 2nd ed.; CRC Press: Boca Raton, FL, USA, 2009.
3. Matsubara, T.; Yaguchi, H.; Takaoka, T.; Jinno, K. *Development of New Hybrid System for Compact Class Vehicles*; SAE Technical Paper: Detroit, MI, USA, 2009. [CrossRef]
4. Brendan, C. *Comparative Analysis of Single and Combined Hybrid Electrically Variable Transmission Operating Modes*; SAE Technical Paper: Detroit, MI, USA, 2005. [CrossRef]
5. Schulz, M. Circulating mechanical power in a power-split hybrid electric vehicle transmission. *Proc. Inst. Mech. Eng. Part D J. Automob. Eng.* **2004**, *218*, 1419–1425. [CrossRef]
6. Ma, C.; Kang, J.; Choi, W.; Song, M.; Ji, J.; Kim, H. A comparative study on the power characteristics and control strategies for plug-in hybrid electric vehicles. *Int. J. Automot. Technol.* **2012**, *13*, 505–516. [CrossRef]
7. Silvas, E.; Hofman, T.; Murgovski, N.; Pascal Etman, L.F.; Steinbuch, M. Review of optimization strategies for system-level design in hybrid electric vehicles. *IEEE Trans. Veh. Technol.* **2017**, *66*, 57–70. [CrossRef]
8. Zhang, X.; Peng, H.; Sun, J. A near-optimal power management strategy for rapid component sizing of power split hybrid vehicles with multiple operating mode. In Proceedings of the American Control Conference (ACC), Washington, DC, USA, 17–19 June 2013.
9. Kim, J.; Kim, N.; Hwang, S.; Hori, Y.; Kim, H. Motor control of input-split hybrid electric vehicles. *Int. J. Automot. Technol.* **2009**, *10*, 733–742. [CrossRef]
10. Hofman, T.; Ebbesen, S.; Guzzella, L. Topology optimization for hybrid electric vehicles with automated transmissions. *IEEE Trans. Veh. Technol.* **2012**, *61*, 2442–2451. [CrossRef]

11. Zhang, X.; Li, C.; Kum, D.; Peng, H. Prius+ and Volt-: Configuration analysis of power-split hybrid vehicles with a single planetary gear. *IEEE Trans. Veh. Technol.* **2012**, *6*, 857–865.

12. Kim, H.; Kum, D. Comprehensive design methodology of compound-split hybrid electric vehicles: In search of optimal configurations. *IEEE Trans. Mechatron.* **2016**, *21*, 2912–2923. [CrossRef]

13. Zhuang, W.; Zhang, X.; Peng, H.; Wang, L. Simultaneous optimization of topology and component sizes for double planetary gear hybrid powertrains. *Energies* **2016**, *9*, 411. [CrossRef]

14. Mashadi, B.; Emadi, S. Dual-mode power-split transmission for hybrid electric vehicle. *IEEE Trans. Veh. Technol.* **2010**, *59*, 3223–3232. [CrossRef]

15. Zhang, X.; Li, S.; Peng, H.; Sun, J. Efficiency exhaustive search of power-split hybrid powertrains with multiple planetary gears and clutches. *J. Dyn. Syst. Meas. Control* **2015**, *137*. [CrossRef]

16. Kang, J.; Choi, W.; Kim, H. Development of a control strategy based on the transmission efficiency with mechanical loss for a dual mode power split-type hybrid electric vehicle. *Int. J. Automot. Technol.* **2012**, *13*, 825–833. [CrossRef]

17. Yang, H.; Cho, S.; Kim, N.; Lim, W.; Cha, S. Analysis of planetary gear hybrid powertrain system part 1: Input split system. *Int. J. Automot. Technol.* **2007**, *8*, 771–780.

18. Kim, N.; Kim, J.; Kim, H. Control strategy for dual-mode electromechanical, infinitely variable transmission for a hybrid electric vehicles. *Proc. Inst. Mech. Eng.* **2008**, *222*, 1587–1601. [CrossRef]

19. Benford, H.; Leising, M. *The Lever Analogy: A New Tool Transmission Analysis*; SAE Paper: Detroit, MI, USA, No. 810102; 1981. [CrossRef]

20. Kim, J. Design and Control of Power Split Transmission for a Hybrid Electric Vehicle. Ph.D. Thesis, Sungkyunkwan University, Seoul, Korea, 2009.

21. Rydh, C.J.; Sanden, B.A. Energy analysis of batteries in photovoltaic systems. Part II: Energy return factors and overall battery efficiencies. *Energy Convers. Manag.* **2005**, *46*, 1980–2000. [CrossRef]

22. Son, H.; Kim, H. Development of near optimal rule-based control for plug-in hybrid electric vehicles taking into account drivetrain component losses. *Energies* **2016**, *9*, 420. [CrossRef]

23. Kim, I.; Kim, H. Configuration Analysis of plug-in hybrid systems using global optimization. In Proceedings of the Electric Vehicle Symposium and Exhibition (EVS27), Barcelona, Spain, 17–20 November 2013.

24. Haka, R.J. Determination of efficiency (torque related losses) in planetary gearsets-generalized theory for simple and compound gearsets. In Proceedings of the ASME 2003 International Design Engineering Technical Conferences and Computers and Information in Engineering Conference, Chicago, IL, USA, 2–6 September 2003; pp. 1085–1097.

25. Chen, J.Y.; Borgerson, J.B. Analytical and test evaluation of planetary gear train efficiency (torque related losses) with multiple power flow arrangements. In Proceedings of the ASME 2003 International Design Engineering Technical Conferences and Computers and Information in Engineering Conference, Chicago, IL, USA, 2–6 September 2003; pp. 1057–1065.

26. *Gears—Thermal Capacity—Part 2: Thermal Load-Carrying Capacity*; ISO/TR 14179-2:2001; International Organization for Standardization: Geneva, Switzerland, 2001.

27. SKF General Catalogue. Available online: http://www.worldcat.org/title/skf-general-catalogue/oclc/225258275 (accessed on 13 January 2016).

28. Changenet, C.; Velex, P. A model for the prediction of churning losses in geared transmissions-preliminary results. *J. Mech. Des.* **2006**, *129*, 128–133. [CrossRef]

29. Yamazaki, K.; Watari, S. Loss analysis of permanent-magnet motor considering carrier harmonics of pwm inverter using combination of 2-D and 3-D finite-element method. *IEEE Trans. Magn.* **2005**, *41*, 1980–1983. [CrossRef]

30. Yuan, Y.; Liu, E.A.; Hill, J.; Zou, Q. An improved hydrodynamic model for open wet transmission clutches. *J. Fluids Eng.* **2007**, *129*, 333–337. [CrossRef]

31. Kirk, D.E. *Optimal Control Theory: An Introduction*; Dover Publications, Inc.: Mineola, NY, USA, 1970.

32. Wang, X.; He, H.; Sun, F.; Zhang, J. Application study on the dynamic programming algorithm for energy management of plug-in hybrid electric vehicles. *Energies* **2015**, *8*, 3225–3244. [CrossRef]

33. Kim, N. Energy Management Strategy for Hybrid Electric Vehicles Based on Pontryagin's Minimum Prinsiple. Ph.D. Thesis, Seoul National University, Seoul, Korea, 2009.

34. Vinot, E.; Trigui, R.; Cheng, Y.; Espanet, C.; Bouscayro, A. Improvement of an EVT-based HEV using dynamic programming. *IEEE Trans. Veh. Technol.* **2014**, *63*, 40–50. [CrossRef]

35. Karbaschian, M.A.; Söffker, D. Review and comparison of power management approaches for hybrid vehicles with focus on hydraulic drives. *Energies* **2014**, *7*, 3512–3536. [CrossRef]
36. Li, Y.; Kar, N.C. Advanced design approach of power split device of plug-in hybrid electric vehicles using dynamic programming. In Proceedings of the Vehicle Power and Propulsion Conference (VPPC), Chicago, IL, USA, 6–9 September 2011.